Hindawi
Shock and Vibration
Volume 2017, Article ID 1402301, 15 pages
https://doi.org/10.1155/2017/1402301

Research Article

Study on the Stiffness Correction Method of Novel Antivibration Bearing for Urban Rail Transit Viaduct

Weiping Xie,[1,2] Youfu Du,[2] Liangming Sun,[1,2] Agostino Marioni,[3] and Xu Liang[2,3]

[1] *Hubei Key Laboratory of Roadway Bridge & Structure Engineering, Wuhan University of Technology, Wuhan 430070, China*
[2] *School of Civil Engineering and Architecture, Wuhan University of Technology, Wuhan 430070, China*
[3] *Wuhan Hirun Engineering Equipment Co., Ltd., Wuhan 430084, China*

Correspondence should be addressed to Liangming Sun; sunliangming@126.com

Received 30 April 2017; Revised 20 July 2017; Accepted 29 August 2017; Published 18 October 2017

Academic Editor: Lutz Auersch

A novel antivibration bearing is developed to reduce the train-induced vibrations for urban rail transit viaduct. It adopts four high-damping thick rubber blocks stacking slantingly to reduce the vibration and provide large lateral stiffness. But the existing stiffness calculation method of laminated rubber bearing aimed at horizontal seismic isolation is unsuitable for thick rubber bearing designed for vertical vibration reduction. First, the stiffness correction method has been proposed based on the characteristics of the novel bearing. Second, to validate the design method, mechanical property tests are performed on a specimen of the novel bearing with design frequency at 8 Hz and with 3500 kN bearing capacity. Third, damping effects of the novel bearing are investigated through impulse vibration tests on scaled models. Results show that the mechanical property of the novel bearing can satisfy the engineering demand, and the proposed method for calculating the stiffness agrees well with the test results. The overall insertion loss of the novel bearing is 13.49 dB which is 5.32 dB larger than that of steel bearing, showing that the novel bearing is very promising to be used in the field to mitigate train-induced vibrations.

1. Introduction

Using viaduct as its main structure, rail transit connects the main cities or economic regions. It plays a vital role in the public transportation. Train-induced bridge vibrations will propagate to the subsoil via the bearings, piers, and foundations and then spread to the surroundings, causing the vibration of surrounding ground, the secondary vibration of adjacent buildings, and its associated structural noise. Since most elevated rail lines close to or even run across the densely populated areas and high-tech industrial parks in cities, the vibration will not only affect the structural safety of the adjacent ancient buildings and people's normal life, but also may have a serious impact on the normal use of that vibration-sensitive high precision instruments in the nearby hospitals, schools, and research institutions [1]. Mitigating at the vibration source and along the vibration propagation path are two major ways to circumvent such train-induced vibrations problem [2]. At the vibration source, the train-bridge system shall be treated sophisticatedly with focus on the vibration mitigation. Elastic track structure [3], tuned mass dampers [4], and fluid viscous dampers [5] are common countermeasurements applied in the field. But the design is sophisticated and costly. The other way is to control the vibration along propagation path. Open or in-filled trenches [6, 7], barriers of piles [8–10], and wave impedance blocks [11, 12] are found to be adopted to mitigate vibrations. But the construction is difficult and site conditions are restricted. Therefore, economical and effective countermeasures are being urgently sought.

The bridge bearing, which connects the superstructure and piers, is on the route of the train-induced vibration propagation and plays a key role as the target of vibration control. But most existing bridge bearings are renowned for their

antiseismic function, such as laminated rubber bearings [13], SMA-based rubber bearings [14], and fiber-reinforced rubber bearings [15]. Those bearings have deficient performance of vertical vibration mitigation because of the high compression stiffness. Considering the dominant direction of the train-induced vibration is vertical, retrofits have to be done on the existing rubber bearings.

To mitigate the train-induced vibrations, elastic bearing pad (EBP) with the assorted shear key (SK) as the supported system of the bridge has been applied to about 5 km of Taiwan high speed railway [16]. Later, this kind of antivibration bearing was also adopted by the Yichang Yangtze River Railway Bridge in Yichang-Wanzhou Railway and the Minjiang River Railway Bridge in Fuzhou-Xiamen Railway to reduce the train-induced vibrations [17]. Sun et al. [18] testified the damping effect of EBP and pot rubber bearing when trains are running on the Yichang Yangtze River Railway Bridge. Tests result showed that the overall insertion loss between the upper and lower plates for EBP and pot rubber bearing was 13.40 dB and 9.65 dB, respectively, and EBP could reduce more vertical train-induced vibrations than pot rubber bearing in most frequency components.

Li et al. [19, 20] analyzed the effect of elastic bearings on train-induced vibrations by simulating the elastic bearings as spring-damper elements. The results showed that the stiffness of elastic bearings had marginally influenced wheel unloading rate and the vertical acceleration of the vehicle, because the elastic bearings could absorb the vibrations in the medium and high frequency bands and amplify their own vibration of natural frequency band. Besides, most researches [21–25] about the elastic bearings were simulated as spring elements to explore the impact of the dynamic responses of vehicle-bridge interaction system. For example, Kawatani et al. [21] analyzed dynamic responses of vehicle-bridge interaction system of certain highway bridge with steel bearings compared to that with elastic bearings based on numerical simulation method. The results showed that elastic bearings could effectively reduce the high frequency vibration. Through the theoretical analysis, Yang et al. [23, 24] studied the impact on dynamic responses of vehicle-bridge interaction system exerted by elastic bearings under moving train loads. The results indicated that the elastic bearings could prevent the transmission or dissipation of vehicle-induced forces from the superstructure to the ground, causing the huge amount of train-induced vibrations energy accumulated and amplified on the bridge during its passage.

The above works indicated that elastic bearing with certain flexibility in vertical direction can reduce the train-induced vertical vibrations transferred to the substructure. Currently, only EBP has been preliminarily applied to mitigate train-induced vibrations, but it must assort SK to resist lateral load because of its small horizontal stiffness. Therefore, based on the attenuation mechanism of antivibration bearing, a novel antivibration bearing with four high-damping thick rubber blocks stacking slantingly is proposed to mitigate vertical vibrations in this paper. Compared with EBP, the novel bearing can mitigate the train-induced vertical vibrations more effectively and provide a large lateral stiffness to limit the lateral displacement caused by train braking or turning at a high speed. The straight forward design of such rubber bearing with low manufacturing costs makes the device promising to be used in the field.

Yabana and Matsuda [26] and He et al. [27] conducted mechanical property tests on thick rubber bearing. Results showed that large compression deformation of thick rubber bearing would be produced under design pressure and the calculation method of compression stiffness of laminated rubber bearing aimed at horizontal seismic isolation was not suitable for thick rubber bearing. Therefore, the calculation of stiffness of the novel bearing with thick rubber blocks must be corrected. Considering the novel antivibration bearing is modeled linearly in the train-bridge interaction system, the stiffness correction method based on multiple iterations with design compression displacement has been proposed. To validate the design method of the novel bearing, mechanical property tests are performed on a specimen. Finally, damping effects of the novel bearing are investigated through impulse vibration tests on scaled models.

2. Design of Novel Antivibration Bearing

2.1. Antivibration Mechanism. Rail transit viaduct with antivibration bearing can be treated as mass-spring-damper system. It can mitigate the sensitivity of the substructure to the train-induced vibrations over the superstructure by inserting a simple harmonic oscillator with lower natural frequency [16]. It can be described as antivibration system with single degree of freedom, as shown in Figure 1.

The mass block represents the bridge superstructure. Assume that the mass block and foundation are rigid, and the elastic spring has damping characteristic, m is the mass of the block in the antivibration system, k is spring stiffness, c is viscous damping coefficient, $F(t)$ is external force, and $x(t)$ is vertical vibration displacement of the mass block. When motivated by the external harmonic excitation $F(t) = F_0 \sin(\theta t)$, the motion equation of the mass block is

$$m\ddot{x}(t) + c\dot{x}(t) + kx(t) = F_0 \sin(\theta t). \tag{1}$$

Based on the theory of structural dynamics [28], the transmissibility coefficient of the antivibration system is

$$T = \frac{\sqrt{1 + (2\xi\beta)^2}}{\sqrt{(1-\beta^2)^2 + (2\xi\beta)^2}}, \tag{2}$$

where $\beta = \theta/\omega$ is the frequency ratio, θ is the circular frequency of the external harmonic excitation, ω is the natural circular frequency of the system, and ξ is the damping ratio.

The variation curve of transmissibility coefficient T with the frequency ratio β for discrete values of the damping ratio ξ is shown in Figure 2. It is indicated that all curves of different damping ratios pass through the same point when frequency ratio $\beta = 2^{1/2}$. Clearly because of this feature, the effectiveness of vibration reduction system will be enhanced by increasing the damping when $\beta < 2^{1/2}$. Similarly, the effectiveness will be decreased by increasing the damping when $\beta > 2^{1/2}$. Since the transmissibility coefficients for $\beta > 2^{1/2}$ are generally much

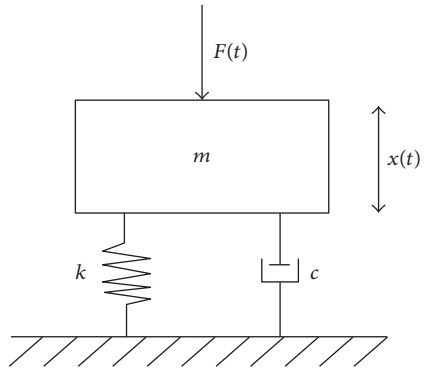

Figure 1: Antivibration system with single degree of freedom.

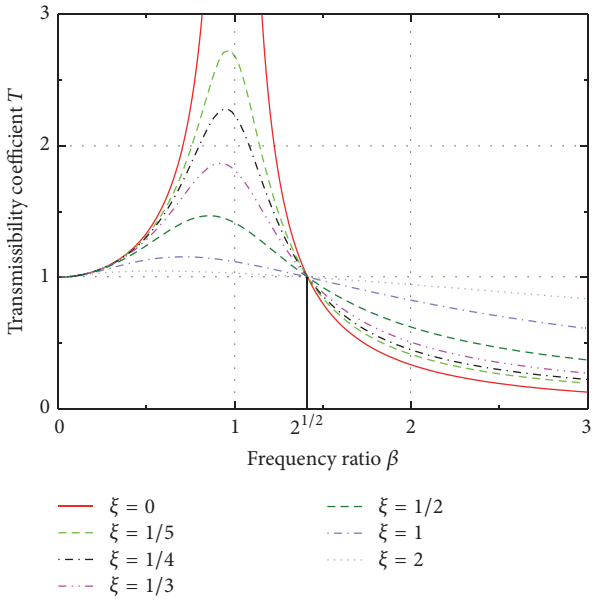

Figure 2: Transmissibility coefficient.

lower than those for $\beta < 2^{1/2}$, it is more efficient to apply countermeasurements at the region with high frequency ratio. However, this is not always practical because the system must operate below $\beta = 2^{1/2}$ in many cases for some intervals of time, and in many other cases it may even operate near the resonant condition $\beta = 1$. Consequently, the principle of vibration mitigation is to increase the frequency ratio as much as possible by decreasing natural frequency of the vibration system, meanwhile to provide proper damping for the bearing to avoid the resonance.

2.2. Design Method. The novel antivibration bearing is designed for urban rail transit viaduct with simply supported box girder. The main type of train used in Chinese urban rail transit is Type-B metro vehicle, and its distance between bogies in the same carriage (L_c) or adjacent carriages (L_b) is 12.6 m or 19 m while between the axles (L_a) it is 2.2 m. Considering the normal operating speed as 60 km/h, the range of variation of the train excitation frequencies is from 0.88 Hz to 7.58 Hz. Therefore, it is appropriate to control the vertical natural frequency of the bridge around 8–10 Hz by proper designing the compression stiffness of the novel bearing, which can efficiently avert from the train excitation frequencies and the noise frequency of the upper structure (10–100 Hz). Generally, the antivibration bearing is modeled linearly in the train-bridge interaction system; thus its natural frequency f (Hz) can be calculated based on the deflection D (m) of bridge structure under static load if the damping is ignored (3). And from the load-deformation curve obtained through the mechanical property test, the compression stiffness of the bearing can be estimated.

$$f = \frac{\sqrt{g}}{2\pi\sqrt{D}} \approx \frac{1}{2\sqrt{D}}, \tag{3}$$

where g is the gravitational acceleration.

From (3), the natural frequency of the antivibration bearing can be decreased with the increase of the deflection of the bridge, but the deflection should not exceed 3-4 mm, or it would impact the serviceability and safety of running train. Hence, the appropriate natural frequency of the novel bearing should be set around 8–10 Hz. But in some cases, the vertical natural frequency of the bridge with the novel bearing may be lower than 8 Hz but generally greater than 4 Hz (depending on the bridge type, mass, and span length). It overlaps with the axis frequency but is far greater than the bogie frequency. Actually, the axle frequency f_a (v/L_a) exerts less influence on the vibration response of train-bridge interaction system, because the wavelength is short and the energy input from the track is small. The resonance response mainly depends on bogie frequency f_b (v/L_b) or f_c (v/L_c). Considering the maximum speed as 80 km/h, the resonance frequency is less than 1.76 Hz. Thus, only little effects would be conducted on the vibration response of train-bridge interaction system when the natural frequency of the bridge is lower than 8 Hz.

The structure diagrams of novel antivibration bearing are shown in Figure 3 where two rubber blocks are α inclined side by side on the left and another two are laid symmetrically on the right. The value range of α is 20°–70°. The lateral direction of the novel bearing is fixed and the longitudinal direction is moveable. To satisfy the different engineering demand, the novel bearing can be designed in different frequency and bearing capacity by changing the parameters of rubber block. The compression stiffness of the novel bearing can ensure the vertical capacity of urban rail transit viaduct and reduce the bridge deflection under dynamic load. Certain horizontal stiffness in lateral direction can limit the lateral displacement caused by extra horizontal load when train is braking or turning at a high speed, ensuring the safety and stability of running trains. And smaller horizontal stiffness in longitudinal direction can ensure the longitudinal displacement of the bridge caused by thermal effect of girder. The application of novel antivibration bearing can increase the frequency ratio β by decreasing the circular natural frequency ω of the bridge, and thus the frequency ratio β can be adjusted to the damping range to meet the expected damping effect.

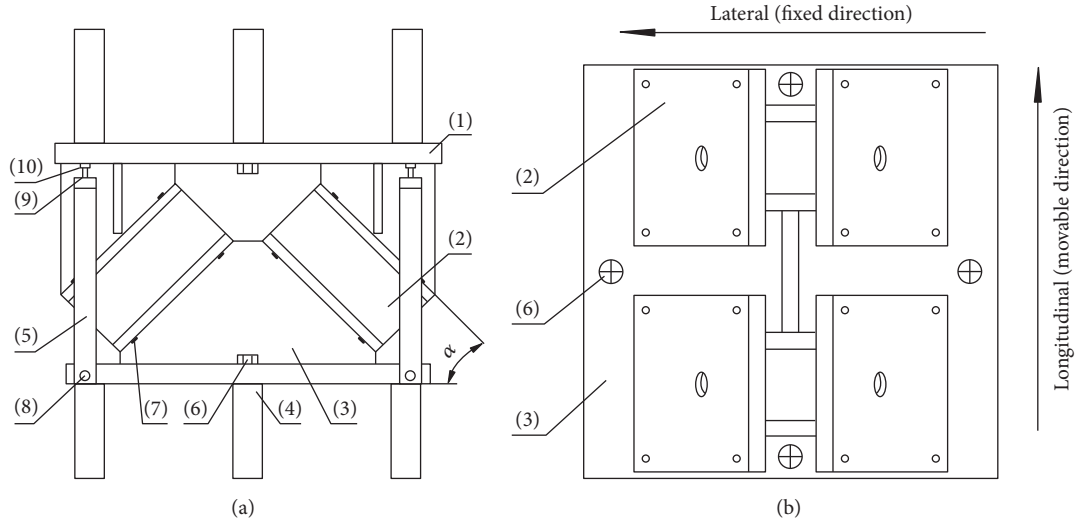

Figure 3: The structure diagram of novel antivibration bearing: (a) front view and (b) relative location arrangement diagram of rubber blocks. *Notes*. (1) Upper plate; (2) high-damping thick rubber block; (3) lower plate; (4) anchor stud; (5) connection plate; (6)~(9) bolt; (10) nut.

2.3. Stiffness Correction Method

2.3.1. Stiffness Calculation for Single Rubber Block. The effective size of rubber block that constitutes the novel bearing is $a \times a$. Based on Chinese national standard GB20688.2-2006 [29], the shape coefficient of the rubber block is

$$S_1 = \frac{a}{4t_r}$$
$$S_2 = \frac{a}{nt_r}, \tag{4}$$

where t_r is the thickness of single layer rubber and n is number of rubber layers.

Horizontal equivalent stiffness is

$$K_h = \frac{GA}{nt_r}, \tag{5}$$

where G is the shear modulus of rubber and A is effective loaded area of rubber block.

Compression stiffness is

$$K_V = \frac{E_c A}{nt_r}, \tag{6}$$

where E_c is the compression elasticity modulus of rubber and the empirical equation $E_c = 3G(1 + 2S_1^2)$ is adopted in this paper [30].

2.3.2. Stiffness Calculation for Novel Antivibration Bearing. Based on the composition and separation of mechanics, the compression stiffness of the novel bearing can be calculated through the mechanical calculation model:

$$K_N = \left(K_V \cos^2\alpha + K_h \sin^2\alpha\right) \times 4. \tag{7}$$

Horizontal equivalent stiffness in longitudinal direction is

$$K_{h1} = 4K_h. \tag{8}$$

Horizontal equivalent stiffness in lateral direction is

$$K_{h2} = \left(K_V \sin^2\alpha + K_h \cos^2\alpha\right) \times 4, \tag{9}$$

where α is vertical inclination angle of rubber block.

2.3.3. Stiffness Correction. The stiffness calculation equations of rubber bearings are all based on design pressure P_0 in the test methods of elastomeric seismic-protection isolators [31]. Different from the laminated rubber bearing aimed at horizontal seismic isolation, the thick rubber bearing has thick single layer rubber, and thus the restraining effect from the internal steel plate to the rubber layer is weaker. Weaker restraints would cause smaller compression stiffness and large compression deformation would be expected under design pressure P_0. Therefore, for the thick rubber bearing, the effect of large compression deformation on the shape coefficient cannot be ignored in the stiffness calculation. Since the novel bearing is composed of thick rubber blocks, its stiffness calculation method must be corrected.

Four thick rubber blocks of the novel bearing will have compression deformation and shear deformation simultaneously under design pressure P_0 as shown in Figure 4. The compression deformation of each rubber block is $d\cos\alpha$ and the shear deformation is $d\sin\alpha$ when compression displacement of the novel bearing is d. The deformation of single layer rubber is shown in Figure 5, where $d_v = d\cos\alpha/n$ and $d_h = d\sin\alpha/n$. The shape coefficient S_1 will increase with the decrease of t_r caused by compression deformation, and the effective loaded area A will decrease by shear deformation.

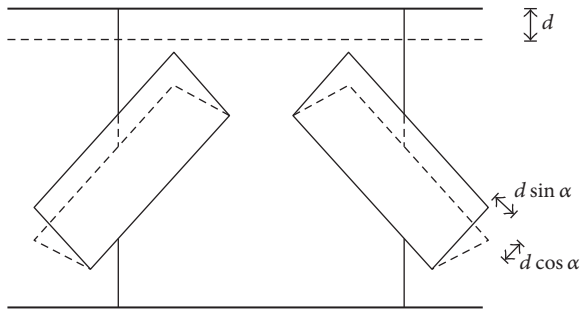

Figure 4: Deformation of the novel bearing under compression load.

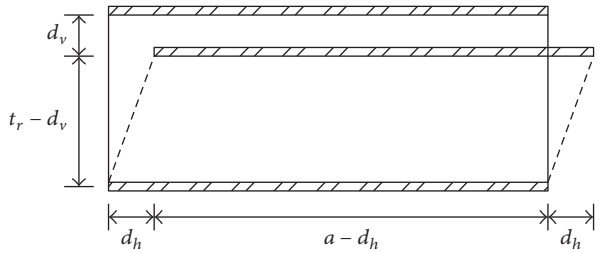

Figure 5: Deformation of single layer rubber.

Therefore, the horizontal equivalent stiffness of single rubber block is corrected as

$$K_h' = \frac{GA}{n\left(t_r - d_v\right)}. \tag{10}$$

Shape coefficient S_1 will turn into

$$S_1' = \frac{a}{4\left(t_r - d_v\right)}. \tag{11}$$

Compressive elasticity modulus E_c will turn into

$$E_c' = 3G\left(1 + 2S_1'^2\right). \tag{12}$$

Compression area of single layer rubber will turn into

$$A' = a \times \left(a - d_h\right). \tag{13}$$

And compression stiffness is corrected as

$$K_V' = \frac{E_c' A'}{n\left(t_r - d_v\right)}. \tag{14}$$

Putting the corrected horizontal equivalent stiffness and compression stiffness of single rubber block into calculation equations (7)–(9), the corrected stiffness of the novel bearing can be calculated.

Therefore, to carry out stiffness correction of the novel bearing, the compression displacement d under design pressure P_0 must be confirmed at first. Considering the novel antivibration bearing is modeled linearly in the train-bridge interaction system, d_1 can be obtained through dividing the design pressure P_0 by the original compression stiffness K_V, and K_{V1} can be obtained based on d_1, $d_2 = P_0/K_{V1}, \ldots$, and then the value of d will tend toward stability after multiple iterations, and it will be utilized to correct the stiffness of the novel bearing. Besides, the displacement d can be confirmed through compression test.

Table 1: Design parameters of the specimen of the novel bearing.

Rubber block	
Rubber hardness	60
Shear modulus G (MPa)	0.8
Effective size $a \times a$ (mm)	300 × 300
Overall thickness (mm)	99.5
Primary shape factor S_1	4.55
Secondary shape factor S_2	6.06
Specimen of the novel bearing	
Frequency (Hz)	8
Vibration damping ratio ξ	10%
Vertical capacity (kN)	3500
Lateral capacity (kN)	700
Lateral displacement (mm)	±0
Longitudinal displacement (mm)	±50

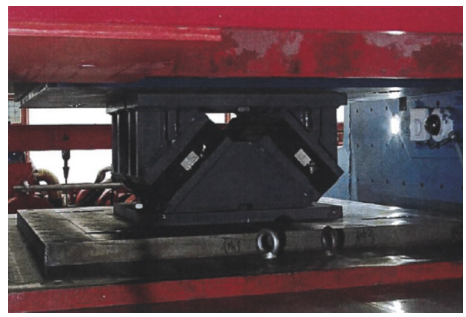

Figure 6: Test specimen of novel antivibration bearing.

3. Mechanical Property of Novel Antivibration Bearing

3.1. Specimen and Testing Apparatus. To validate the design method, mechanical property tests are performed on a specimen of the novel bearing with design natural frequency at 8 Hz and with 3500 kN bearing capacity. The design parameters of the specimen are shown in Table 1. The inclination angle α of rubber block is 45°.

The specimen and testing equipment are fixed mechanically through an external fixing plate to avoid the relative sliding between the specimen and test platform, as shown in Figure 6. The mechanical property tests are performed through 75000 kN multipurpose testing machine, as shown in Figure 7. The machine can conduct dynamic control in both vertical and horizontal direction simultaneously. Performance parameters of this testing machine are as follows: vertical dynamic load 75000 kN, horizontal dynamic load

Table 2: Mechanical property test program of novel antivibration bearing.

Test types	Loading direction	Amplitude	Loading frequency/Hz	Loading waveform	Vertical loads/kN	Cycle-index
Compression property	Vertical	/	/	/	3500	3
Shear property	Longitudinal	±50 mm	0.005	/	2600	3
	Lateral	±700 kN	0.2	/	2600	3
Shearing strain correlation	Longitudinal	25 mm	0.5	Sine	2600	3
		50 mm	0.5	Sine	2600	3
		75 mm	0.5	Sine	2600	3
Loading frequency correlation	Longitudinal	50 mm	0.001	Ramp	2600	1
		50 mm	0.005	Ramp	2600	1
		50 mm	0.01	Ramp	2600	3
		50 mm	0.1	Sine	2600	3
		50 mm	0.5	Sine	2600	3
		50 mm	1.0	Sine	2600	3
		50 mm	2.0	Sine	2600	3
Loading times correlation	Longitudinal	50 mm	0.5	Sine	2600	50
Ultimate shear property	Longitudinal	±75 mm	/	/	3500	/

Figure 7: Multifunctional testing machine.

6000 kN, maximum vertical displacement 120 mm, maximum horizontal displacement ±600 mm, and maximum horizontal peak velocity 1000 mm/s.

3.2. Testing Program. The mechanical property tests are strictly performed according to GB/T 20688.1-2007 [31]. Three-cyclic loading of 0-P_{max}-0 will be conducted in vertical direction during the compressive property test, among which P_{max} is maximum design pressure 3500 kN. Displacement loading in longitudinal direction and horizontal load loading in lateral direction are adopted in shear property test. Shear property correlation tests include the correlation of shearing strain, loading frequency, and loading time, which mainly study horizontal mechanical property under varying horizontal deformation. After the correlation tests, the ultimate shear property tests are performed in longitudinal positive direction and negative direction, respectively, to measure the ultimate shear displacement ability of the test specimen under the maximum design pressure. The detailed testing program is shown in Table 2.

3.3. Definition of Mechanical Property Index. The calculation equation of compression stiffness is

$$K_N = \frac{P_2 - P_1}{Y_2 - Y_1}, \tag{15}$$

where P_1 is $0.7P_0$, P_2 is $1.3P_0$, P_0 is the design pressure 2600 kN in normal train operation, and Y_1 and Y_2 are compression displacement corresponding to the third cycle of compression loads P_1 and P_2, respectively.

The equation of horizontal equivalent stiffness is

$$K_h = \frac{Q_1 - Q_2}{X_1 - X_2}, \tag{16}$$

where Q_1 is the maximum shear force, Q_2 is the minimum shear force, X_1 is maximum displacement, and X_2 is minimum displacement.

The equation of horizontal equivalent damping ratio is

$$h_{eq} = \frac{2\Delta W}{\pi K_h (X_1 - X_2)^2}, \tag{17}$$

where ΔW is envelop area of the third cycle of the hysteretic loops.

3.4. Results and Discussion

3.4.1. Compression Property and Shear Property. Compressive load-displacement curve under three-cyclic loading is shown in Figure 8. Based on (15), compression stiffness K_N of the specimen is 479.8 kN/mm, which can ensure the vertical capacity of urban rail transit viaduct.

Horizontal load-displacement curves of the specimen under three-cyclic loading are shown in Figure 9. The horizontal load shown in the figure comprises the actual shearing

Table 3: Comparison among the theoretical stiffness and measured stiffness.

Stiffness	Measured	Standard calculated	Error	Corrected value	Error
K_N (kN/mm)	479.8	372.0	22.5%	471.9	1.7%
K_{h1} (kN/mm)	7.31	5.80	20.7%	6.32	15.7%
K_{h2} (kN/mm)	861.4	372.0	56.8%	471.9	45.2%

Table 4: Test results of K_{h1} in different shear strain.

Shear strain	Q_1 (kN)	Q_2 (kN)	X_1 (mm)	X_2 (mm)	K_{h1} (kN/mm)	Normalization
50%	195.0*	−192.9*	24.59	−24.17	7.96	1.08
100%	366.5*	−359.6	49.36	−49.13	7.37	1.00
150%	505.0*	−503.1*	73.7	−73.6	6.84	0.93

Notes. The value with ∗ is actual shear load which is equal to horizontal load minus the friction of machinery equipment, the same in Tables 5 and 6.

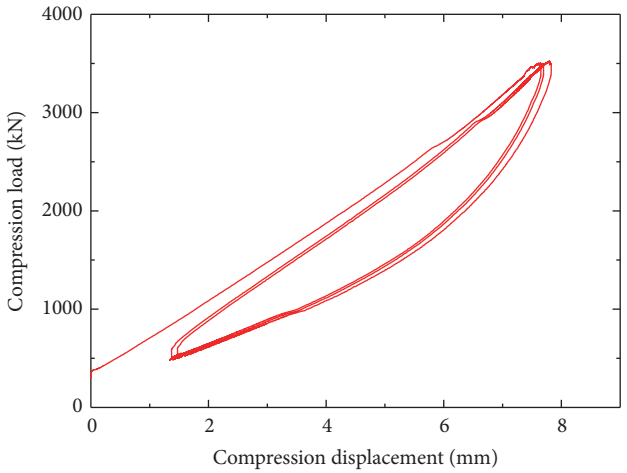

Figure 8: Compressive load-displacement curve under three-cyclic loading.

load and the friction of machinery equipment itself. Then, the actual shearing load is equal to horizontal load minus the friction of machinery equipment. Based on (16), horizontal equivalent stiffness of the specimen in longitudinal direction (K_{h1}) and lateral direction (K_{h2}) is 7.31 kN/mm and 861.4 kN/mm, respectively. Thus, the measured K_{h1} is smaller, which can ensure the horizontal displacement of the longitudinal bridge caused by thermal effect of girder. Based on (17), the equivalent damping ratio h_{eq} in longitudinal direction is 9.6%, showing the specimen possesses great energy-dissipating capacity. Besides, Figure 9(b) indicates that the lateral displacement of the specimen is less than 1 mm when the horizontal load reaches the design lateral bearing capacity 700 kN. It shows that K_{h2} of the specimen is sufficient to resist the expected horizontal load in the lateral direction of bridge and to limit the lateral displacement caused by train braking or turning at a high speed.

The theoretical stiffness of the specimen can be calculated based on the stiffness calculation method mentioned in Section 2.3. It should be noted that the design compression displacement d required for stiffness correction is obtained by trial. The deviation between $d_5 = 5.51$ mm and $d_4 = 5.52$ mm is less than 1%. Thus, the iteration number should be set to 5 and the final design compression displacement d set to 5.51 mm. Figure 8 shows that the measured compression displacement of the specimen is 5.83 mm when the compression load is 2600 kN. The error between measured compression displacement and design compression displacement is only 5.5%. It proves that the design compression displacement after multiple iterations has high precision.

Comparison among the theoretical stiffness and measured stiffness of the specimen is shown in Table 3. It indicates that the error between corrected value and measured value is smaller than that of standard calculated value, whether compression stiffness or horizontal equivalent stiffness. K_{h2} of the specimen is much larger than theoretical value. That is because the lateral deformation is less than 1 mm (shearing strain $\gamma < 2\%$) in the test, and the actual shear modulus is much larger than theoretical value ($\gamma = 100\%$) when γ is minimal. Higher horizontal equivalent stiffness in lateral direction means stronger lateral load resistance to meet the operating requirements better. Since the damping effect of the novel bearing depends mainly on compression stiffness and the error between corrected compression stiffness and measured compression stiffness is only 1.7%, the stiffness correction method is much more consistent with real situation.

3.4.2. Correlation of Shear Property in Longitudinal Direction. The horizontal load-displacement curves of the specimen in different shear strain are shown in Figure 10. And the corresponding test results of K_{h1} are shown in Table 4. It is indicated that K_{h1} decreases with the increase of longitudinal displacement, which agrees with characteristics of the hysteresis loop of high-damping rubber. Based on the shearing strain 100% (50 mm), the variation range of K_{h1} will be 0.93–1.08.

The horizontal load-displacement curves of the specimen in different loading frequency are shown in Figure 11. And the corresponding test results of K_{h1} are shown in Table 5. It is indicated that K_{h1} of the specimen decreases with the increase of loading frequency. Based on the loading frequency 0.5 Hz, the variation range of K_{h1} will be 0.93–1.12.

The loading time correlation test of the specimen requires repetitive loading for 50 times. Considering the capacity of

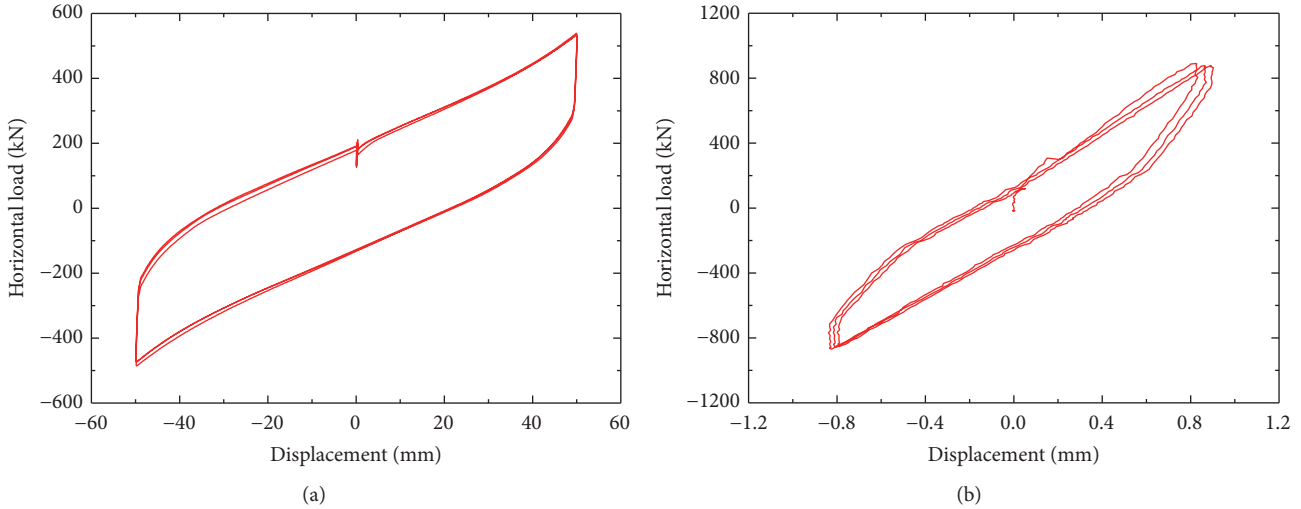

Figure 9: Horizontal load-displacement curves under three-cyclic loading: (a) longitudinal and (b) lateral.

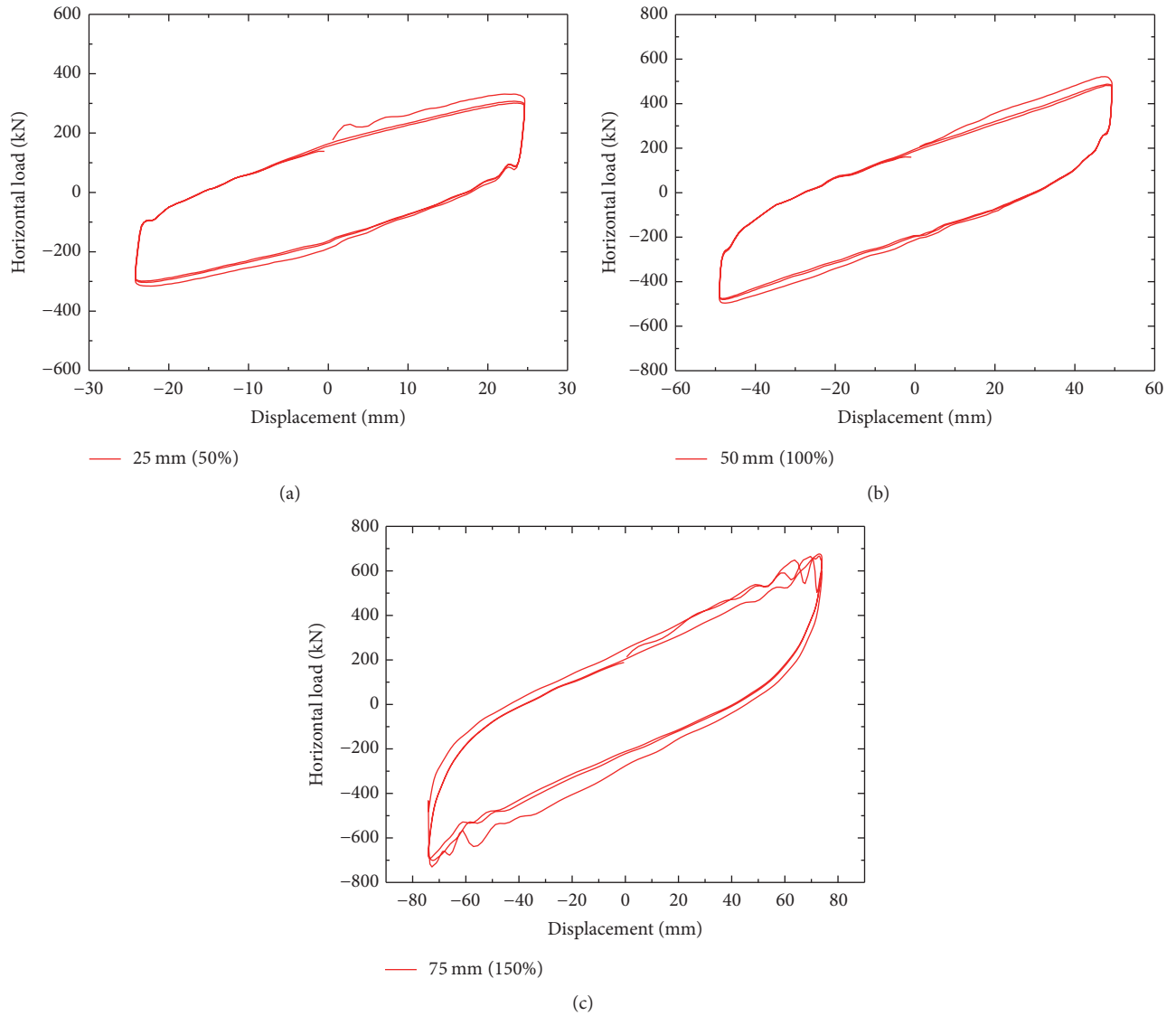

Figure 10: Curves of the shearing strain correlation test: (a) 50%, (b) 100%, and (c) 150%.

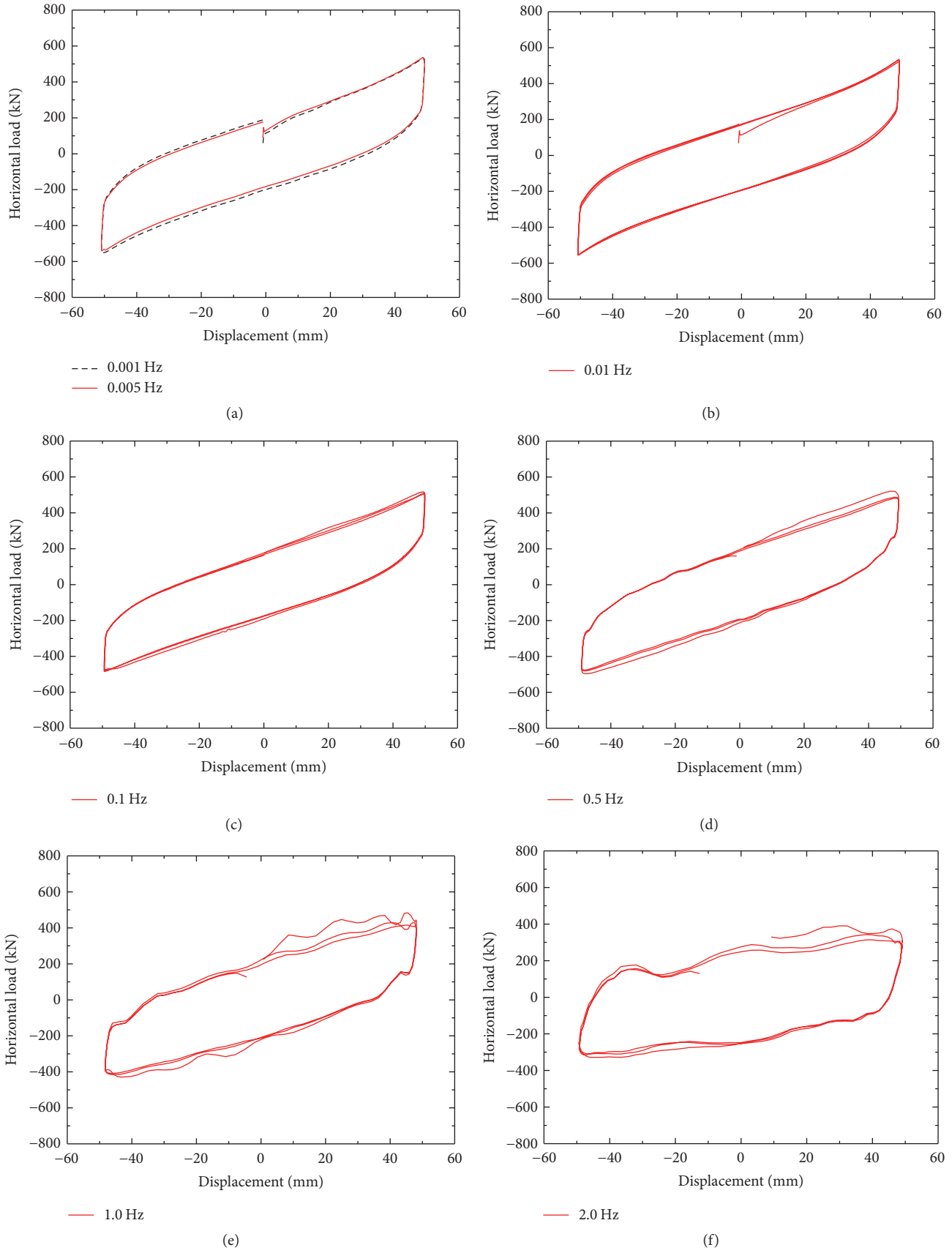

Figure 11: Curves of loading frequency correlation test: (a) 0.001 Hz and 0.005 Hz, (b) 0.01 Hz, (c) 0.1 Hz, (d) 0.5 Hz, (e) 1.0 Hz, and (f) 2.0 Hz.

Table 5: Test results of K_{h1} in different loading frequency.

Frequency (Hz)	Q_1 (kN)	Q_2 (kN)	X_1 (mm)	X_2 (mm)	K_{h1} (kN/mm)	Normalization
0.001	397.3*	−414.4*	49.14	−50.91	8.11	1.12
0.005	398.3*	−404.1*	49.14	−50.93	8.07	1.12
0.01	385.2*	−407.4*	48.97	−50.74	7.96	1.10
0.1	367.6*	−346.5*	49.74	−49.30	7.21	1.00
0.5	357.9*	−350.4*	49.29	−49.00	7.21	1.00
1.0	333.7*	−326.9*	48.14	−48.27	6.85	0.95
2.0	323.3*	−333.4*	49.04	−49.24	6.68	0.93

Table 6: Test results of K_{h1} in different loading times.

Times	Q_1 (kN)	Q_2 (kN)	X_1 (mm)	X_2 (mm)	K_{h1} (kN/mm)	Normalization
1	352.4*	−337.5*	49.23	−49.17	7.01	1.08
3	322.7*	−317.8*	49.21	−49.17	6.51	1.00
5	312.5*	−316.9*	49.19	−49.17	6.39	0.98
10	306.1*	−315.9*	49.17	−49.17	6.32	0.97
30	310.9*	−314.3*	49.96	−49.37	6.29	0.97
50	307.2*	−308.6*	50.20	−49.13	6.20	0.95

Table 7: Similarity relation between model and prototype.

Similarity factor	Symbol	Formula	Value (model/prototype)
Size	S_l	$S_l = l_M/l_P$	0.182
Elastic modulus	S_E	$S_E = E_M/E_P$	1.000
Acceleration	S_a	$S_a = S_E S_l^2/S_m$	1.002
Mass	S_m	$S_m = m_M/m_P$	0.033
Time	S_t	$S_t = (S_l/S_a)^{0.5}$	0.426
Frequency	S_f	$S_f = 1/S_t$	2.347
Displacement	S_u	$S_u = S_l$	0.182
Stress	S_σ	$S_\sigma = S_E$	1.000
Strain	S_ε	$S_\varepsilon = 1$	1.000
Force	S_F	$S_F = S_E S_l^2$	0.033

energy accumulator in testing machine, the loading time correlation test will be conducted for three times with loading cycles 1–15, 16–32, and 33–50 successively. The horizontal load-displacement curves of the specimen under different loading time are shown in Figure 12. And the corresponding test results of K_{h1} are shown in Table 6. It is indicated that K_{h1} decreases with the increase of loading time. Based on the third loading time, the variation range of K_{h1} will be 0.95–1.08.

3.4.3. Ultimate Shear Property in Longitudinal Direction. In ultimate shear property test of the specimen, test picture when shear displacement is +75 mm (150% shear strain) is shown in Figure 13. Test curves of ultimate shear property are described as Figure 14. Results show that the specimen does not have any signs of damage when shear displacement reaches its ultimate value 75 mm under the design bearing capacity, and the shear load monotonously increased with the increase of displacement. It proves that the ultimate shear property of the specimen in longitudinal direction has satisfactory performance.

4. Damping Effects of Novel Antivibration Bearing

4.1. Test Scheme. Damping effects of the novel bearing are investigated through impulse vibration tests on scaled models. The scaled models of the novel bearing and steel bearing are shown in Figure 15. The similarity relation of length ratio between the model and prototype is set as 1/5.5, and their similarity relation is shown in Table 7. It should be noted that the full-scaled specimen of the novel bearing is constituted by four rubber blocks, while scaled model is constituted by two rubber blocks. That is to say, one scaled model of the novel bearing is equivalent to half of scaled bearing specimen according to the similarity relation of length ratio 1/5.5.

4.2. Test Process. The impulse vibration tests of scaled model are performed in Earthquake Engineering Center of

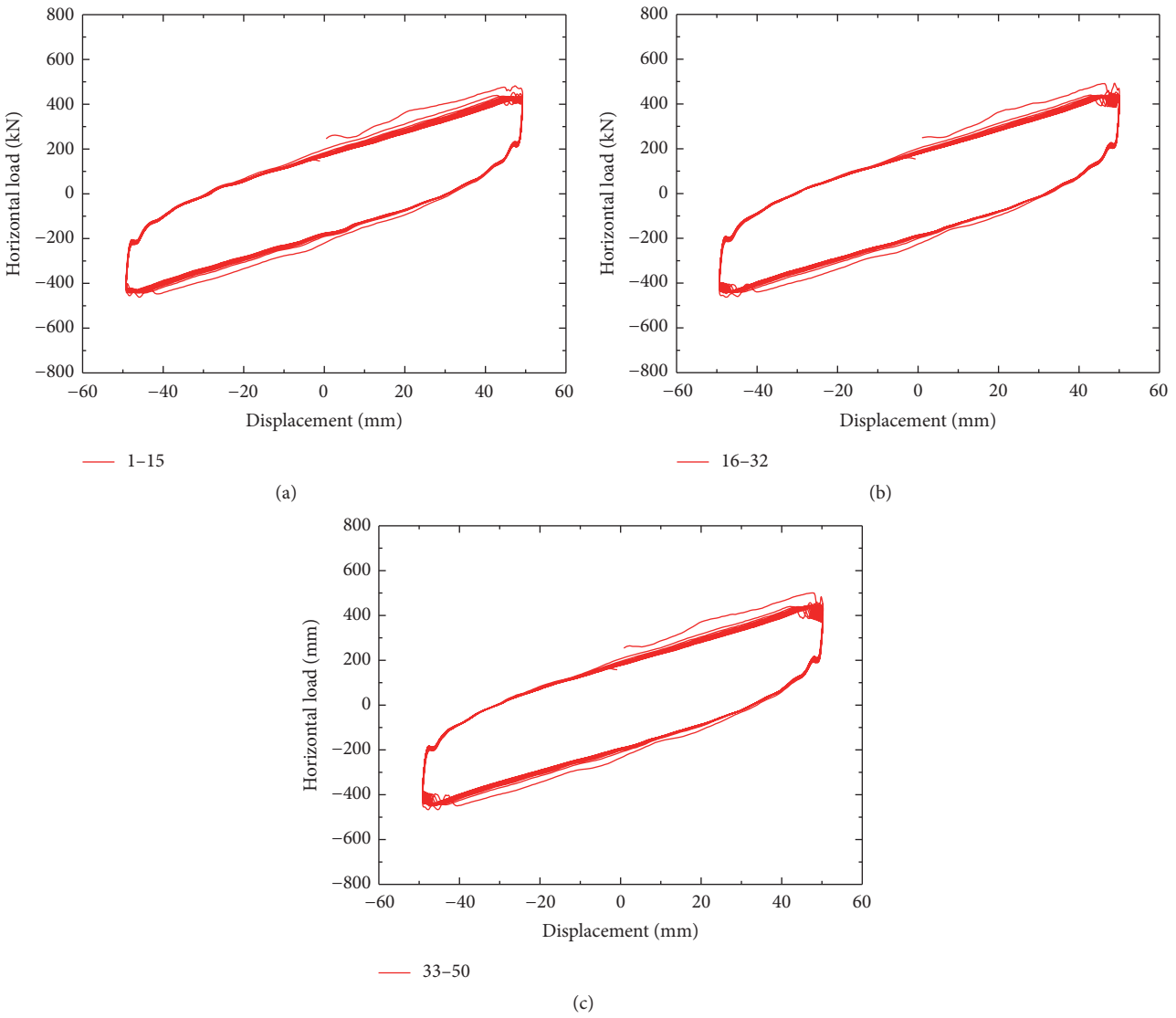

Figure 12: Curves of loading time correlation test: (a) 1–15, (b) 16–32, and (c) 33–50.

Figure 13: Test picture when shear displacement is +75 mm.

Guangzhou University. Test scheme is shown in Figure 16. There are four scaled bearings placed in each corner of the square ground, and every two of them are placed by T-type relations, which is equivalent to two-scaled bearing specimen. Considering design bearing capacity is 2600 kN for the normal train operation, additional weight composed of the concrete and steel slab is 171.6 kN based on the similarity ratio 0.033. Dynamic loads are excited by an electromagnetic vibrator which is placed at the center of slab. Sweep frequency is 5–230 Hz. This test applies four accelerometers to gather vertical acceleration responses as shown in Figure 16, where accelerometer 1 is located at the lower plate of the bearing, accelerometers 2 and 3 are located on the concrete slab, and accelerometer 4 is located on the vibrator.

4.3. Results and Discussion. Under the impulse vibration in vertical direction, the time histories and Fourier spectra of novel antivibration bearing and steel bearing at accelerometer 2 and accelerometer 1 are shown in Figure 17. It is indicated that the maximum acceleration responses of the upper and lower plates in the novel bearing are 0.11 m/s^2 and 0.0048 m/s^2, with main frequency components around 20 Hz or 50–60 Hz. While in steel bearing, the corresponding value

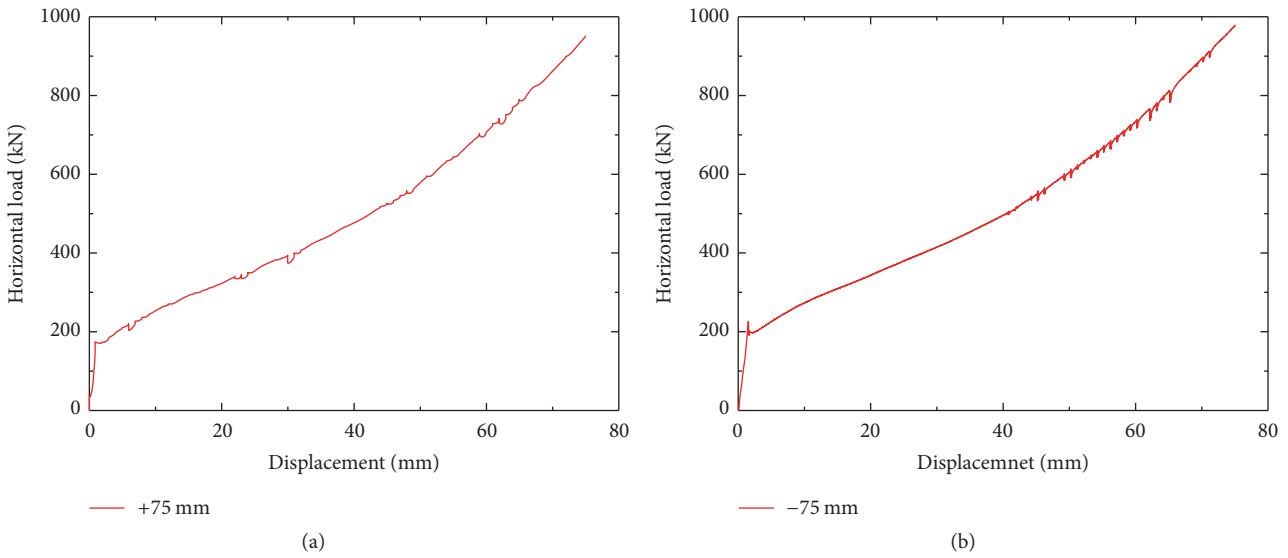

Figure 14: Test curves of ultimate shear property: (a) 75 mm and (b) −75 mm.

Figure 15: Scaled models: (a) novel antivibration bearing and (b) steel bearing.

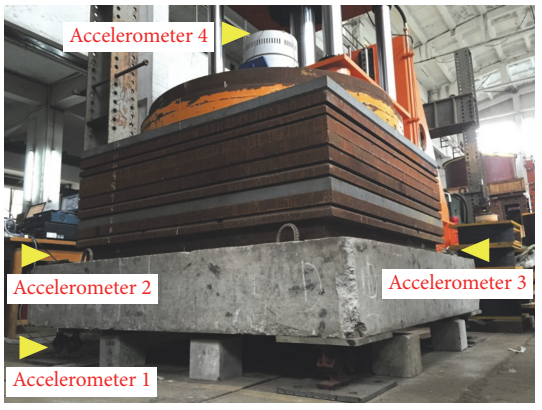

Figure 16: Test scheme of impulse vibration test on scaled models.

of upper and lower plates are 0.073 m/s^2 and 0.0021 m/s^2, with main frequency components around 20–30 Hz or 65–75 Hz.

In accordance with the Chinese national standards GB 1007-1988 [32], the vibration level is defined as follows:

(1) Vibration acceleration level is

$$\mathrm{VAL} = 20 \lg \frac{a_{\mathrm{RMS}}}{a_0}, \tag{18}$$

where $a_0 = 10^{-6}$ m/s^2 is a reference vibration acceleration and a_{RMS} is the vibration acceleration RMS.

(2) Z vibration level is as follows.

Corrected by Z-weighted factor of the whole-body vibration, the vibration acceleration level is noted as VL_Z based on ISO2631/1-1997 [33].

The dominant frequency of vertical ground vibration induced by the passage of trains is 10–100 Hz, and the dominant frequency of transverse vibration is 4–100 Hz [34]. Based on GB 10071-1988 [32], only 1–80 Hz of vertical vibration needs to be assessed. Therefore, 1–80 Hz was adopted to make assessment on the damping effect of the novel bearing. The 1/3 octave band analysis is performed to discuss the vertical Z vibration level in the range of 1–80 Hz. Results show that the average VL_Z of upper and lower plates for the steel bearing are 67.67 dB and 59.50 dB, respectively, and

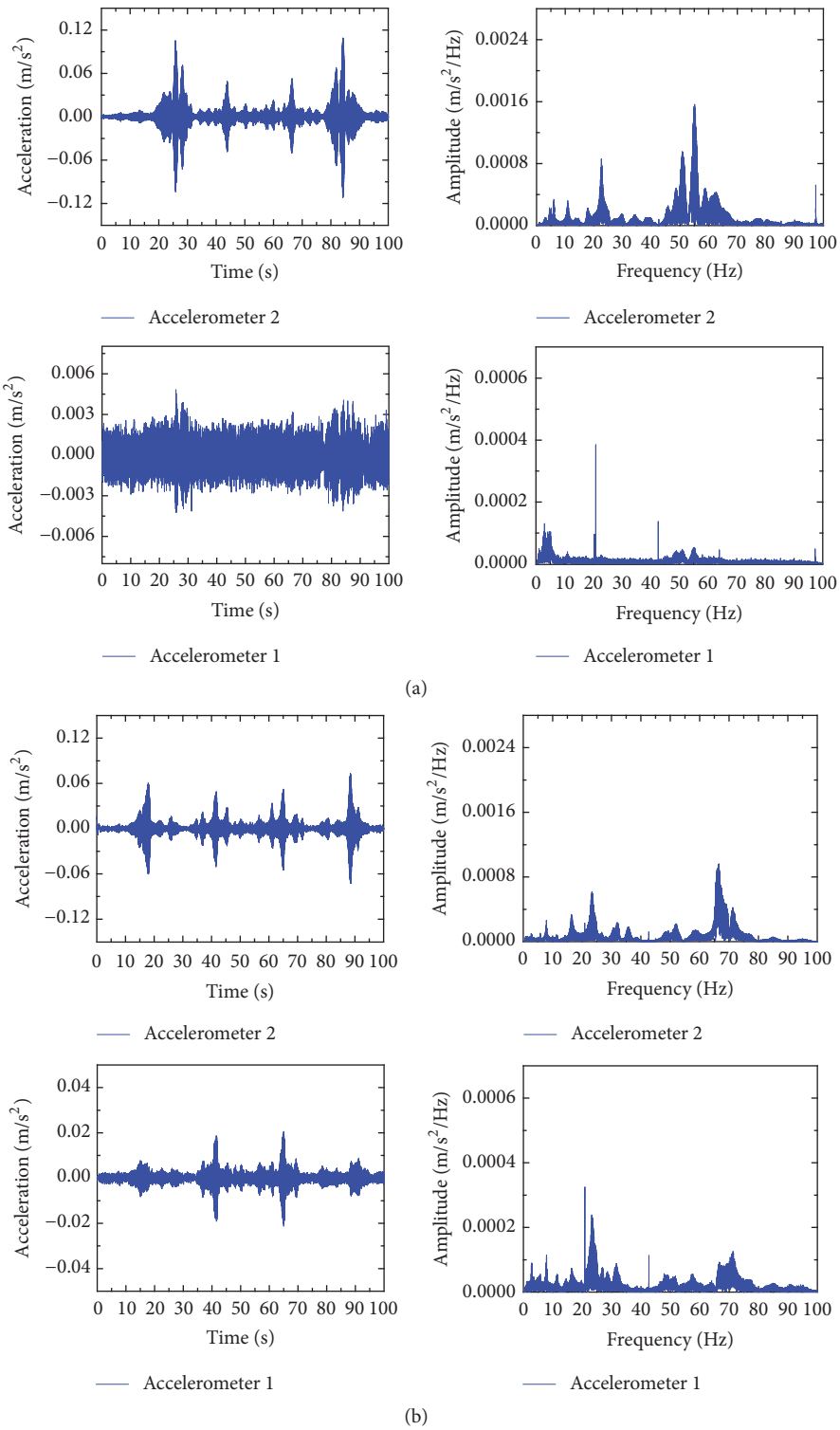

Figure 17: Vertical acceleration time histories and Fourier spectra: (a) novel antivibration bearing and (b) steel bearing.

the whole insertion loss is 8.17 dB, while the average VL_Z of upper and lower plates for the novel bearing are 70.29 dB and 56.80 dB, respectively, and the whole insertion loss is 13.49 dB. Therefore, the overall insertion loss of the novel bearing is 5.32 dB larger than that of steel bearing.

Comparison of the insertion loss for steel bearing and the novel bearing in the frequency domain of 1–80 Hz is shown in Figure 18. From the comparison, both steel bearing and the novel bearing can cause the insertion loss in most frequency components, which shows that both can reduce

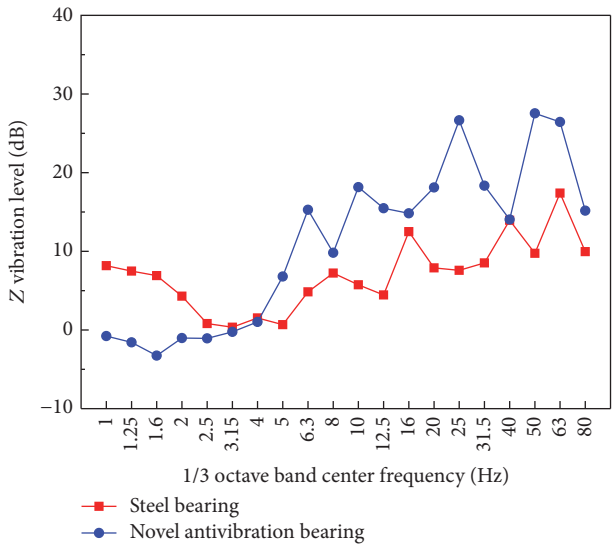

Figure 18: Comparison of the insertion loss for steel bearing and novel antivibration bearing.

certain vertical vibration. However, the vibration responses of the novel bearing are amplified below 1/3 octave band center frequency 4 Hz. That is because the novel bearing as a flexible support decreases the natural frequency of the structure. The vibration responses are mitigated in the medium and high frequency bands and amplified in the low frequency bands. In this sense, the damping effects of the novel bearing is worse than that of the steel bearing below the center frequency 4 Hz. But above the center frequency 4 Hz that contains the main dominant frequency of vertical vibration induced by the passage of trains (10–80 Hz), the novel bearing can reduce more vibrations than the steel bearing. It can be concluded that the novel bearing can effectively mitigate the train-induced vertical vibrations.

5. Conclusion

For the bridge bearing, the principle to mitigate vertical vibration is to increase the frequency ratio by appropriately decreasing natural frequency of the vibration system and also provide proper damping to avoid the resonance. In this paper, a novel antivibration bearing that adopts four high-damping thick rubber blocks stacking slantingly is proposed to reduce vertical vibrations and provide a large lateral stiffness simultaneously. Considering the novel bearing is modeled linearly in the train-bridge interaction system, the associated stiffness correction method is proposed based on multiple iterations with design compression displacement.

To validate the design method, mechanical property tests are performed on a specimen of the bearing device with design natural frequency at 8 Hz and with 3500 kN bearing capacity. Test results show that the measured K_N of the specimen is 479.8 kN/mm, which can ensure the vertical capacity of urban rail transit viaduct; the measured K_{h1} is 7.31 kN/mm, which can ensure the horizontal displacement of the longitudinal bridge caused by thermal effect of girder; the measured K_{h2} is 861.4 kN/mm, which can resist the expected lateral load of bridge. The equivalent damping ratio h_{eq} in longitudinal direction is 9.6%, showing the specimen possesses great energy-dissipating capacity. The tests also prove that the specimen has stable performance in longitudinal direction. Therefore, the mechanical property of the novel bearing can satisfy the engineering demand. The error between corrected value and measured value is smaller than that of standard calculated value, whether compression stiffness or horizontal equivalent stiffness. So, the test results agree well with the prediction of the proposed stiffness correction method.

Damping effects of the novel bearing are investigated through impulse vibration tests on scaled models. When electromagnetic vibrator is operating on test model, it shows that vibration amplitudes of the novel bearing at the upper and lower plates are smaller than those of steel bearing. The whole insertion loss of the novel bearing is 13.49 dB which is 5.32 dB larger than that of steel bearing in the range of 1–80 Hz. The damping effect of the novel bearing is worse than that of the steel bearing below the center frequency 4 Hz because of the vibration amplification effect of flexure supporting structure in the low frequency bands. But above the center frequency 4 Hz that contains the main dominant frequency of vertical vibration induced by the passage of trains (10–80 Hz), the novel bearing can reduce more vibrations than the steel bearing. Therefore, the novel bearing can effectively mitigate the train-induced vertical vibrations and it will benefit the circumvention of the vibration problem along the elevated rail line.

Conflicts of Interest

The authors declare that there are no conflicts of interest regarding the publication of this paper.

Acknowledgments

This work was supported by the National Natural Science Foundation of China (51608410), Hubei Provincial Natural Science Foundation of China (2016CFB272), Hubei Key Laboratory of Roadway Bridge and Structure Engineering (Wuhan University of Technology) (DQJJ201505), and the Fundamental Research Funds for the Central Universities (2016IVA028 and 2017-zy-062).

References

[1] S. Yokoshima and A. Tamura, "A study on factors constituting annoyance due to Shinkansen railway vibration," *Journal of Architecture, Planning and Environmental Engineering*, vol. 64, no. 526, pp. 1–7, 1999.

[2] S. Lakušić and M. Ahac, "Rail traffic noise and vibration mitigation measures in urban areas," *Technical Gazette*, vol. 19, no. 2, pp. 427–435, 2012.

[3] G. Lombaert, G. Degrande, B. Vanhauwere, B. Vandeborght, and S. François, "The control of ground-borne vibrations from railway traffic by means of continuous floating slabs," *Journal of Sound and Vibration*, vol. 297, no. 3-5, pp. 946–961, 2006.

[4] J. F. Wang, C. C. Lin, and B. L. Chen, "Vibration suppression for high-speed railway bridges using tuned mass dampers," *International Journal of Solids and Structures*, vol. 40, no. 2, pp. 465–491, 2003.

[5] M. D. Martínez-Rodrigo, J. Lavado, and P. Museros, "Dynamic performance of existing high-speed railway bridges under resonant conditions retrofitted with fluid viscous dampers," *Engineering Structures*, vol. 32, no. 3, pp. 808–828, 2010.

[6] L. Andersen and S. R. K. Nielsen, "Reduction of ground vibration by means of barriers or soil improvement along a railway track," *Soil Dynamics and Earthquake Engineering*, vol. 25, no. 7–10, pp. 701–716, 2005.

[7] M. Adam and O. Von Estorff, "Reduction of train-induced building vibrations by using open and filled trenches," *Computers and Structures*, vol. 83, no. 1, pp. 11–24, 2005.

[8] J. Avilés and F. J. Sánchez-Sesma, "Foundation isolation from vibrations using piles as barriers," *Journal of Engineering Mechanics*, vol. 114, no. 11, pp. 1854–1870, 1988.

[9] G. Y. Gao, Z. Y. Li, C. Qiu, and Z. Q. Yue, "Three-dimensional analysis of rows of piles as passive barriers for ground vibration isolation," *Soil Dynamics and Earthquake Engineering*, vol. 26, no. 11, pp. 1015–1027, 2006.

[10] P.-H. Tsai, Z.-Y. Feng, and T.-I. Jen, "Three-dimensional analysis of the screening effectiveness of hollow pile barriers for foundation-induced vertical vibration," *Computers and Geotechnics*, vol. 35, no. 3, pp. 489–499, 2008.

[11] H. Takemiya and A. Fujiwara, "Wave propagation/impediment in a stratum and wave impeding block (WIB) measured for SSI response reduction," *Soil Dynamics and Earthquake Engineering*, vol. 13, no. 1, pp. 49–61, 1994.

[12] H. Takemiya, "Field vibration mitigation by honeycomb WIB for pile foundations of a high-speed train viaduct," *Soil Dynamics and Earthquake Engineering*, vol. 24, no. 1, pp. 69–87, 2004.

[13] T. H. Kim, Y. J. Kim, and H. M. Shin, "Seismic performance assessment of reinforced concrete bridge piers supported by laminated rubber bearings," *Structural Engineering and Mechanics*, vol. 29, no. 3, pp. 259–278, 2008.

[14] A. R. Bhuiyan and M. S. Alam, "Seismic performance assessment of highway bridges equipped with superelastic shape memory alloy-based laminated rubber isolation bearing," *Engineering Structures*, vol. 49, no. 2, pp. 396–407, 2013.

[15] H. Zhang, J. Li, and T. Peng, "Development and mechanical performance of a new kind of bridge seismic isolator for low seismic regions," *Shock and Vibration*, vol. 20, no. 4, pp. 725–735, 2013.

[16] Marioni, L. Chen, and J. T. Hu, "Application of EBP on Taiwan high-speed railway," *Earthquake Resistant Engineering and Retrofitting*, vol. 33, no. 2, pp. 63–66, 2011.

[17] X. Y. Hu and G. Z. Yu, "Brief discussion about bridge vibration isolation bearing products," in *Proceedings of the fifth nationwide rubber products technical seminar, Rubber cup in Donghai*, pp. 79–84, Ningbo, China, 2009.

[18] L. M. Sun, W. P. Xie, and W. He, "Field measurement on vibration reduction effects of anti-vibration bearings for vertical train-induced vibrations," in *Proceedings of the Fourteenth International Symposium on Structural Engineering, Fundamental Research in Structural Engineering: Retrospective and Prospective*, pp. 982–988, Beijing, China, 2016.

[19] Z. J. Zhang, X. Z. Li, X. Zhang et al., "Study on the vibration isolation effects of elastic bearings on train-induced vibration of railway bridge," *Engineering Mechanics*, vol. 32, no. 4, pp. 103–111, 2015.

[20] X. Li, Z. Zhang, and X. Zhang, "Using elastic bridge bearings to reduce train-induced ground vibrations: An experimental and numerical study," *Soil Dynamics and Earthquake Engineering*, vol. 85, pp. 78–90, 2016.

[21] M. Kawatani, Y. Kobayashi, and H. Kawaki, "Influence of elastomeric bearings on traffic-induced vibration of highway bridges," *Transportation Research Record: Journal of the Transportation Research Board*, vol. 1696, pp. 76–82, 2000.

[22] C.-W. Kim, M. Kawatani, and W.-S. Hwang, "Reduction of traffic-induced vibration of two-girder steel bridge seated on elastomeric bearings," *Engineering Structures*, vol. 26, no. 14, pp. 2185–2195, 2004.

[23] J.-D. Yau, Y.-S. Wu, and Y.-B. Yang, "Impact response of bridges with elastic bearings to moving loads," *Journal of Sound and Vibration*, vol. 248, no. 1, pp. 9–30, 2001.

[24] Y. B. Yang, C. L. Lin, J. D. Yau, and D. W. Chang, "Mechanism of resonance and cancellation for train-induced vibrations on bridges with elastic bearings," *Journal of Sound and Vibration*, vol. 269, no. 1-2, pp. 345–360, 2004.

[25] T. Jiang, C. Y. Ma, and X. Zhang, "Dynamic analysis of train-bridge system with elastic supports," *Chinese Quarterly of Mechanics*, vol. 25, no. 2, pp. 256–263, 2004.

[26] S. Yabana and A. Matsuda, "Mechanical properties of laminated rubber bearings for three-dimensional seismic isolation," in *Proceedings of the 12th World Conference on Earthquake Engineering*, 2000.

[27] W. F. He, W. G. Liu, Y. F. Yang et al., "The basic mechanical properties of thick rubber isolators," *Journal of PLA University of Science and Technology (Natural Science Edition)*, vol. 12, no. 3, pp. 258–263, 2011.

[28] R. Clough and J. Penzien, *Structural of Dynamics*, Computers & Structures, Inc., USA, 3rd edition, 1995.

[29] GB 20688.2-2006, *Rubber Bearings-Part 2: Elastomeric seismic-protection isolators for bridges*, China Standards Press, Beijing, China, 2006.

[30] EN 15129-2009, Anti-seismic devices, 2009.

[31] GB/T 20688.1-2007, *Rubber Bearings-Part 1: Seismic-protection isolators test methods*, China Standards Press, Beijing, China, 2006.

[32] GB 10071-1988, *Measurement Method of Environmental Vibration of Urban Area*, National Environmental Protection Agency, China, 1988.

[33] ISO 2631/1-1997, *Mechanical Vibration and Shock: Evaluation of Human Exposure to Whole-Body Vibration-Part 1: General Requirements*, 1997.

[34] X. Z. Li, Q. M. Liu, X. Zhang et al., "Ground vibration induced by inter-city express train," *Journal of Vibration and Shock*, vol. 33, no. 16, pp. 56–61, 2014.